

# Stereo-crossed ablation guided by stereoelectroencephalography for epilepsy: comprehensive coagulations *via* a network of multi-electrodes

Peng-Hu Wei, Xiao-Tong Fan, Yi-He Wang, Chao Lu, Si-Qi Ou, Fei Meng, Mu-Yang Li, Hua-Qiang Zhang, Si-Chang Chen, Yang An, Yan-Feng Yang, Lian-Kun Ren, Yong-Zhi Shan  and Guo-Guang Zhao

*Ther Adv Neurol Disord*

2020, Vol. 13: 1–13

DOI: 10.1177/  
1756286420928657

© The Author(s), 2020.  
Article reuse guidelines:  
sagepub.com/journals-  
permissions

## Abstract

**Background:** Introducing multiple different stereoelectroencephalography electrodes in a three-dimensional (3D) network to create a 3D-lesioning field or stereo-crossed radiofrequency thermocoagulation (scRF-TC) might create larger lesioning size; however, this has not been quantified to date. This study aimed to quantify the configurations essential for scRF-TC.

**Methods:** By using polyacrylamide gel (PAG), we investigated the effect of electrode conformation (angled/parallel/multiple edges) and electrode distance of creating an electrode network. Volume, time, and temperature were analyzed quantitatively with magnetic resonance imaging, video analysis, and machine learning. A network of electrodes to the pathological left area 47 was created in a patient; the seizure outcome and coverage range were further observed.

**Results:** After the compatibility test between the PAG and brain tissue, the sufficient distance of contacts (from different electrodes) for confluent lesioning was 7 mm with the PAG. Connection to the lesioning field could be achieved even with a different arrangement of electrodes. One contact could achieve at least six connections with different peripheral contacts. Coagulation with a network of electrodes can create more significant lesioning sizes, 1.81–2.12 times those of the classic approaches. The confluent lesioning field created by scRF-TC had a volume of 38.7 cm<sup>3</sup>; the low metabolic area was adequately covered. The representative patient was free of seizures throughout the 12-month follow up.

**Conclusion:** Lesioning with electrodes in a network manner is practical for adequate 3D coverage. A secondary craniotomy could be potentially prevented by combining both monitoring and a large volume of lesions.

**Keywords:** epilepsy, radiofrequency thermocoagulation, stereoelectroencephalography, stereo-crossed

Received: 3 December 2019; revised manuscript accepted: 28 April 2020.

## Introduction

As an approach to ablate the intracranial lesions, traditional stereotactic radiofrequency thermocoagulation (RF-TC) was introduced more than half a century ago,<sup>1</sup> and it has long been used to treat epileptic patients.<sup>2–5</sup> When the limitations of the

canonical stereotactic radiofrequency apparatus, that is, its inability to record electrical information, became apparent, stereoelectroencephalography (SEEG) electrodes were introduced to facilitate the radiofrequency procedure in the past two decades.<sup>6–9</sup> However, through either the

Correspondence to:

**Yong-Zhi Shan**  
Department of  
Neurosurgery, Xuan  
Wu Hospital, Capital  
Medical University, No. 45  
Changchun Street, Xuanwu  
District, Beijing 100053,  
China

[shanyongzhi@xwhosp.org](mailto:shanyongzhi@xwhosp.org)

**Guo-Guang Zhao**  
Department of  
Neurosurgery, Xuanwu  
Hospital, Capital Medical  
University, Beijing, 100053,  
China

[ggzhao@vip.sina.com](mailto:ggzhao@vip.sina.com)

**Peng-Hu Wei**  
**Xiao-Tong Fan**  
**Yi-He Wang**  
**Chao Lu**  
**Si-Qi Ou**  
**Fei Meng**  
**Mu-Yang Li**  
**Hua-Qiang Zhang**  
**Si-Chang Chen**  
**Yang An**

**Yan-Feng Yang**  
Department of  
Neurosurgery, Xuanwu  
Hospital, Capital Medical  
University, Beijing, China

**Lian-Kun Ren**  
Department of Neurology,  
Xuanwu Hospital, Capital  
Medical University, Beijing,  
China

traditional approach or the novel SEEG-guided approach, the clinical outcome was consistently shown to be unsatisfactory due to the relatively small lesioning size.<sup>3,9</sup> To explore how to expand the lesioning field, studies were carried out *in vitro* with albumen in recent years.<sup>10,11</sup> While these studies advocated the importance of coagulation from a pair of distant contacts,<sup>11</sup> knowledge of RF-TC still rests on low-dimensional space with a limited number of contacts, making full coverage of natural epileptogenesis challenging.

Should the lesioning field be expanded by integrating multiple contacts to coagulate in a network manner, that is, stereo-crossed RF-TC (scRF-TC)? After preliminary albumen and animal investigations,<sup>12</sup> our recent studies have shown that, with this design, seizure outcomes in patients with hypothalamic hamartomas and hippocampal sclerosis were improved without a secondary craniotomy.<sup>8,12</sup> To further quantify the characteristics of scRF-TC that are important to the clinical practice from bed to the bench, it is necessary to address the constraints of albumen as a liquid. Specifically, in the scRF-TC, if the configurations and distances of the deformable electrodes are to be calibrated by holding the electrodes more stably, a semi-solid phantom would be better. Besides, the uncontrollable ventilation of a liquid phantom that might take heat away from the contacts must be averted.<sup>13</sup> Furthermore, the lesioning field in albumen is vulnerable to further positional change, and this limits the application of magnetic resonance imaging (MRI) in three-dimensional (3D) volumetric evaluation. Thus, a novel phantom is required in the study.

Among explorations of thermocoagulation, as a semi-solid phantom, polyacrylamide gel (PAG) was proposed to mimic human tissues.<sup>14-17</sup> This phantom might overcome the shortcomings of albumen. Therefore, the present study aimed to first determine between PAG and albumen as the better phantom for RF-TC of the brain, and then the excellent one will go on to be preferred for further scRF-TC study. We also analyzed the size of the lesion in humans and compared it with lesioning fields in PAG. Special configurations, such as the effect of electrode conformation (angled/parallel/multiple edges) and electrode distance in creating an electrode network, were also quantified in the present study.

## Methods

In the present study, we investigated which is the better phantom between PAG and egg albumen. The recipes and preparation process for PAG have been shown previously.<sup>17</sup> Retrospective cases were compared with *in vitro* phantoms. SEEG electrodes (Alcis, Besançon, France) and a radiofrequency lesion generator (R-2000B, Beijing Neo Science Co., Ltd., Beijing, China) were used to create the lesioning field. The lesioning areas in albumen were evaluated by coordinate grids (Supplemental Figure S1), whereas the fields in PAG and retrospective cases were assessed according to high-resolution MRI. After the superior phantom was determined, videos of the coagulation *in vitro* were used to quantify the size evolution across time, and temperature distributions were further quantified *via* a machine learning technique. Conformations (angled/parallel/multiple edges) of the electrodes in creating a lesioning network were quantified. Figure 1 presents the general design of the present study. This study was approved by the ethical committee of Xuanwu Hospital (LYS-[2019]-097).

### Reliability evaluation of the phantoms

**Test-retest repetitiveness.** With the same manipulations and parameters (2 W, 3 W, and 4 W in 30 s, 60 s, and 90 s, respectively), the repeatability of diameters in PAG and repeatability of diameters in egg albumen (Supplemental Figure S1) were compared using intraclass correlation coefficients (ICCs). Differences across different coagulations in each of the phantom are presented as mean  $\pm$  standard deviation. The more stable phantom would be further compared with *in vivo* data of rodents and retrospective humans.

**In vitro, animal, and human data comparisons.** To determine the comparability of the phantom with tissues in rats and humans under the same conditions (power: 3 W, duration: 60 s), by using the size index of the “diameter vertical to the electrode,” we compared results generated with neighboring contacts in the more stable phantom and the lesioning field in two rats (executed at 7 days after RF-TC), as well as three retrospective patients (measured from MRI scanned within 6 h after RF-TC) with hypothalamic hamartoma.

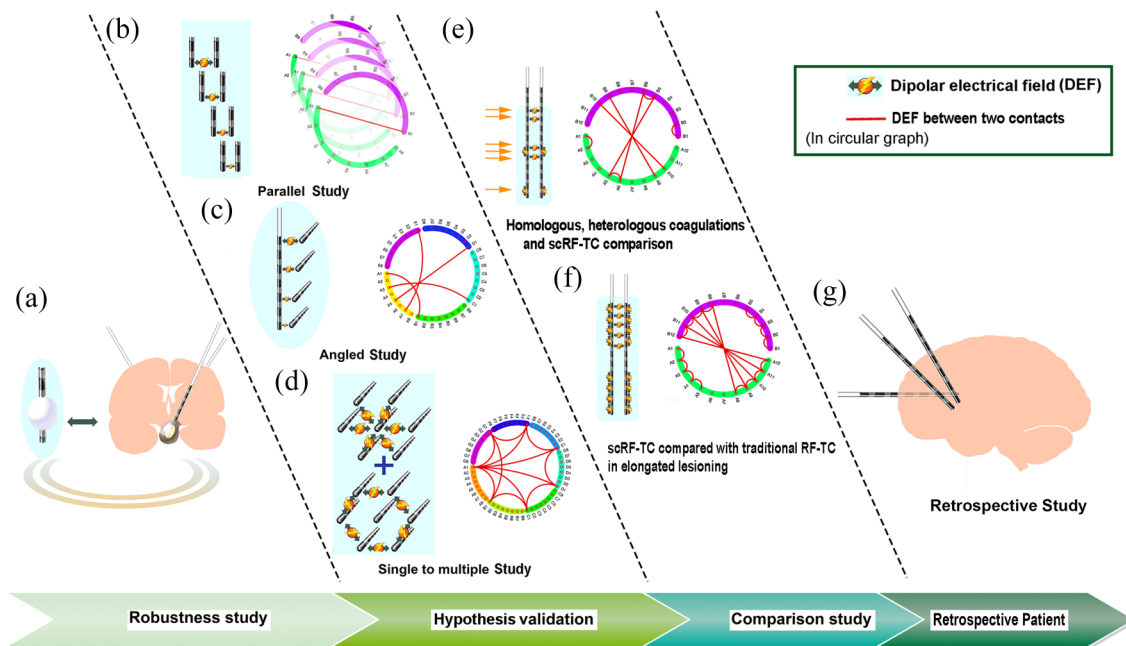


**Figure 1.** Schematic drawing of the study design. (a) Robustness study: carried out to test the repeatability and compatibility of the polyacrylamide gel. (b) Parallel study: parallel electrodes were placed at distances of 3 mm, 5 mm, 7 mm, and 9 mm, through which RF-TCs are performed. (c) Vertical study: vertical electrodes arrayed at distances of 3 mm, 5 mm, 7 mm, and 9 mm to perform RF-TCs. (d) Single-to-multiple study: the central contact coagulated with each peripheral contact, respectively, followed by each peripheral coagulated with each other. (e) Comparison of homologous, heterologous coagulations, and scRF-TC; (f) scRF-TC versus traditional RF-TC in elongated lesioning; (g) Retrospective study: ablate epileptogenesis in a human in whom the seizure outcome as observed. RF-TCs, radiofrequency thermocoagulations; scRF-TC, stereo-crossed radiofrequency thermocoagulations.

### *Effective distance, electrode orientations, and one-to-multiple contacts in vitro*

To quantify how a 3D physiological network could be created, three properties were needed, considering these questions: (1) What are the distances of the contacts that are valid for creating a confluent lesioning field? (2) Could the coagulation process be performed through distant electrodes of “different arrangements”? (3) Are multiple connections applicable from one contact to multiple contacts?

For the distance and arrangement tests, coagulations were performed with contact distances of 3 mm, 5 mm, 7 mm, and 9 mm, either from a pair of parallel electrodes or a pair of vertical electrodes (the most extreme situation of being not parallel). For the one-to-multiple coagulations, one electrode was placed at the center, and six other electrodes were placed around the central electrode at 7 mm or 9 mm away in a hexagonal shape. Parameters of 3 W and 150 s were used.

The central contact was used repetitively six times to pair with each vertex contact, one by one, for coagulation, and the vertex contacts were then required to coagulate with each adjacent contact, one by one (Figure 1). Quantitative evaluation of the time, size, and temperature distribution were performed further (presented in *Data acquisition and analysis*).

### *Effective investigation in vitro and retrospective studies*

*In vitro studies.* Here, we defined homologous and heterologous coagulations as coagulation from contacts of the same and different electrodes, respectively (Figure 1). Typically, the scRF-TC is constituted of both homologous coagulations and heterologous coagulations. In this session of experiments, quantitative analyses of size and temperature distribution were evaluated using three strategies: first, purely with homologous coagulations; second, solely with

parallel heterologous coagulations; and third, scRF-TC, which combined the previous homologous and parallel heterologous coagulations simultaneously. Four contacts were adopted, as the lowest number that could achieve all three combinations of contacts.

As is the case during clinical practice, RF-TC is typically performed in a continuous manner<sup>10</sup>; we therefore compared the effects of continuous scRF-TC with continuous traditional RF-TC. A pair of 12-contact electrodes was implanted in parallel into the PAG. The lower five contacts in each electrode (10 contacts from the two electrodes) were used consecutively for homologous coagulations, whereas the upper five contacts of each electrode were involved in both homologous and parallel heterologous coagulations in scRF-TC. Size and temperature distribution were further analyzed quantitatively.

*Retrospective studies.* A 23-year-old female patient with frontal lobe seizure was enrolled. The patient had experienced seizures approximately twice a month over the last 7 years, and she manifested a right deviation of the head and mouth at seizure onset, severe spasm of the right eyelid, and tight closing of the right eye. These symptoms were followed by a convulsion of all four limbs with clenching of both fists. Seconds later, the patients' head and mouth would deviate to the left, and this would last until the end of the seizure. The entire seizure lasted for 2–3 min and was accompanied by loss of consciousness. The patient could not recall the seizure afterward.

MRI findings were negative. However, positron emission tomography (PET) revealed a region of low metabolism in Brodmann's areas 46 and 47 in the frontal lobe [presumed seizure onset zone (presumed SOZ)] (Figure 2a). Although similar regions of low metabolism were found in other lobes, scalp electroencephalography, and magnetoencephalography, which were conducted as a confirmation of symptomatology, both suggested a left frontal origin. Thus, low metabolic regions in other lobes were excluded as presumed SOZs.

To perform scRF-TC, 11 electrodes were implanted (Figure 2b), with seven located in the presumed SOZ. Of these seven electrodes, one was inserted anteriorly to posteriorly and penetrated the center of the presumed SOZ (electrode I), whereas the other six electrodes were oriented

vertically, arranged from left to right, and distributed both superior (electrodes SA, SM, and SP) and inferior (electrodes IA, IM, and IP) to the horizontal electrode. scRF-TC was performed with these electrodes; the duration was 60 s, and a power of 3 W was delivered (the rationale of the parameters is described in the *Discussion*).

The lesioning size was calculated based on the 3D reconstruction of an MRI rechecked 2 h after scRF-TC. A comparison between the lesioning area and the low metabolism area was made by registering the MRI recheck data to the preoperative PET data. The seizure outcome was evaluated using the Engel classification.

#### *Data acquisition and analysis*

For most of the experiments in PAG, a guiding screw was embedded vertically into a cuboid piece of rubber, and the distances between the electrodes were defined by applying methylene blue to the surface of the PAG as a marker. The rubber was fixed to the frame of the container. A Kirschner wire fitted with a screw holder to define the implantation distance was used to create a trajectory *via* the guiding screw in the cuboid rubber. PAG samples with apparent deviations observed in the MRI scan were removed from the analysis to guarantee reliability.

*PAG embedding in gelatin for MRI scanning.* Gelatin powder was dissolved in water at 80°C to create a 15% solution of gelatin. The embedding process was kept at a temperature of less than 28°C. The specimen was kept on ice during transport.

*MRI acquisition.* MRI was performed in a 3-T MRI scanner with a 20-channel coil (3T Siemens PRISMA, Siemens, Erlangen, Germany). For the T1 sequence, the parameters were as follows: voxel size, 0.7 mm iso; matrix size, 300 × 252 × 240; TR, 2110 ms; TE, 2.3 ms; flip angle, 0°. For the turbo T2-weighted spin-echo sequence, we used the following parameters: voxel size, 0.7 mm iso; matrix size, 320 × 320 × 256; TR, 3200 ms; TE, 563 ms; flip angle, 0°.

#### *Data processing*

*MRI preprocessing of PAG data.* For high-quality analysis, several data preprocessing steps were essential. We first applied a bias field correction to all T1 and T2 images with the N4ITK MRI Bias Correction module in the software 3D



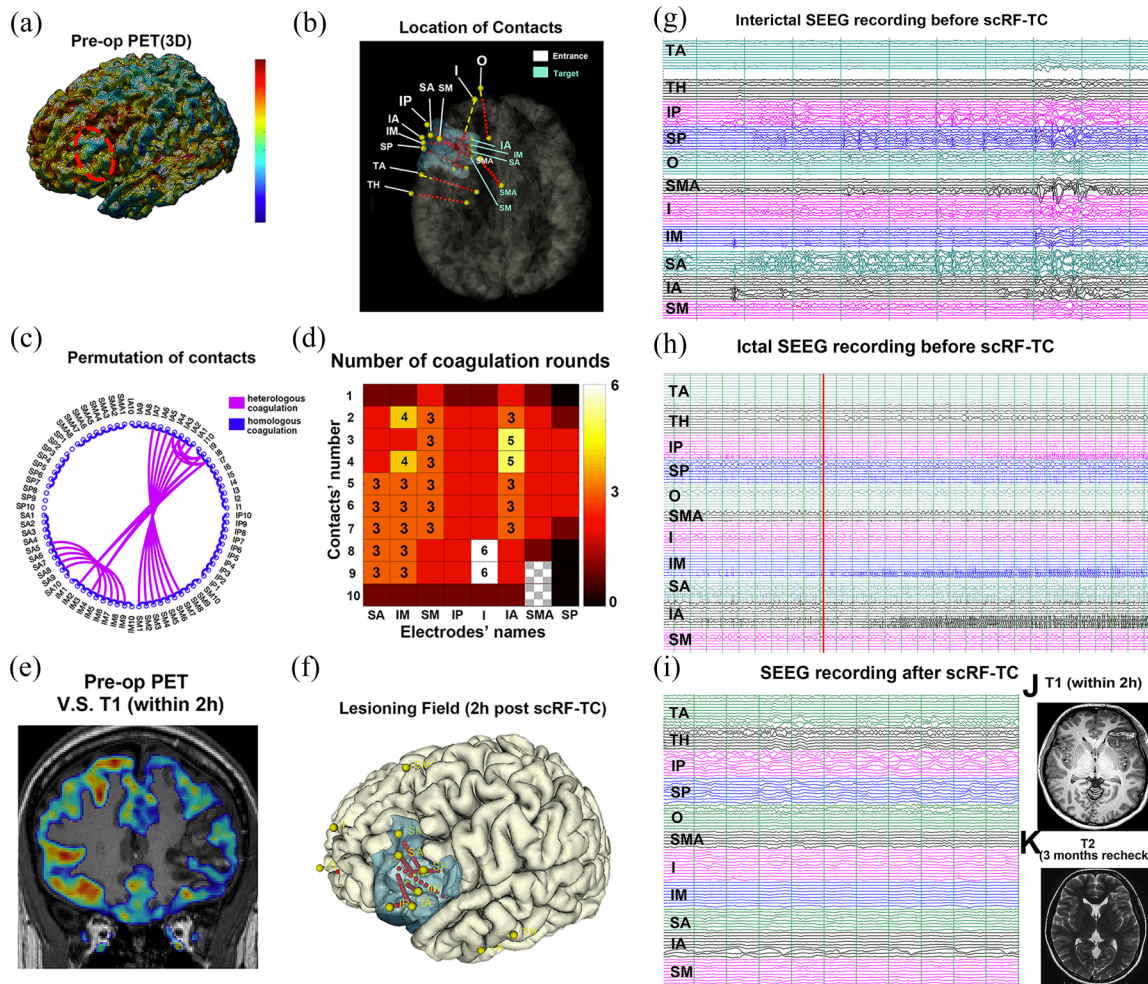


**Figure 2.** Validation of *in vitro* results in a clinical case. (a) 3D reconstruction of the preoperative PET–MRI data reveal a prominent region of low metabolism (red circle) located in the left frontal lobe. (b) Locations of the contacts based on a postimplantation CT scan. (c) A circular graph illustrates the lesioning plan, where purple represents heterologous lesioning, and blue represents homologous lesioning. (d) A matrix plot showing the number of coagulation rounds, in which contacts I8 and I9 underwent six rounds of coagulations. (e) MRI at 2h after scRF-TC treatment showing that the low-metabolism area on the PET scan was covered adequately by the lesioning field. (f) 3D reconstruction based on MRI performed 2h after treatment indicates that the volume of the lesioning field (blue) reached 38.7 ml. (g) Interictal SEEG recordings revealed massive spike and slow waves in multiple channels. (h) Ictal SEEG recordings indicated a seizure discharge originated from the cortical contacts in the electrode IM. (i) Posttreatment stereoelectroencephalography showing elimination of the epileptic discharges shown in (g). (j) MRI performed 2h after treatment shows the comprehensive lesioning field. (k) A 3-month follow-up MRI indicates the residual lesioning field and absorption of the microhematomas.

CT, computed tomography; 3D, three-dimensional; MRI, magnetic resonance imaging; PET, positron emission tomography; scRF-TC, stereo-crossed radiofrequency thermocoagulations; SEEG, stereoelectroencephalography.

Slicer (<https://download.slicer.org>). Then, all data were averaged by adjusting the mean of the values across different trials to the same standard amount using MATLAB (The MathWorks, Inc., Natick, MA, USA). To facilitate further temperature analysis with machine learning, we defined this standard value with a piece of uncoagulated

PAG embedded together with the model from the water-bath experiment.

*Quantifying the 3D volumes.* The 3D volumes were based on masks using the intensity of the T2 signal with the segment editor module in the 3D Slicer software, in which the profile of the lesioning

field was more clearly outlined. Volumes were calculated by multiplying the number of voxels of the mask by the volume of a single voxel in MATLAB.

*Temperature classified with machine learning.* The PAG was separated into small uncovered pieces (size: 9.5 mm × 9.5 mm × 24 mm), and each piece was immersed in water with temperatures ranging from 44°C to 83°C for 1 min. Thus, each piece corresponded to one temperature, with a total of 40 pieces representing 40 temperatures (Supplemental Figure S2). These PAGs were also embedded in gelatin for further MRI scanning. As each piece of the PAG corresponded to approximately 6300 voxels, we obtained 6300 T1 values and 6300 T2 values corresponding to each temperature. With a decision tree model (in MATLAB), we used the T1 and T2 values as the predictor and temperatures as the response to create a classifier. Further analysis of the temperature distribution was based on this classifier. As protein denaturation and coagulation necrosis occur at 57–60°C,<sup>18</sup> special attention was paid to areas where the temperature is above 60°C.

*Quantitative analysis of the video data.* Video data analysis was performed using MATLAB software. As the 0–140 s is consistent of high quality for analysis across different videos, videos of this duration were adopted to analyze the size evolution. To facilitate further investigation, we first converted the RGB coordinates of each pixel into a grayscale system to assign a single value to each pixel, where this value approximately reflects the opacity of the PAG, except for the vertical experiments, in which the shadows of electrodes influenced the value in a relatively complex arrangement. The degree of opacity in a pixel was defined as the grayscale value of the pixel divided by the maximum grayscale value with that coagulation process.

*Reconstruction of the electrodes in the patient.* The locations of the contacts were determined by computed tomography (CT) after electrode implantation. The CT data were co-registered to the preoperative T1 scan using SPM software (<https://www.fil.ion.ucl.ac.uk/spm/software/download/>). The coordinates of each contact were decoded using the SEEG Assistant module (<https://github.com/mnarizzano/SEEGA>) in 3D Slicer.

*Estimation of lesion volume in the patient.* Cortical parcellation of T1 images was performed

before and after thermocoagulation using the FreeSurfer software (<https://surfer.nmr.mgh.harvard.edu/fswiki/DownloadAndInstall>), in which healthy brain tissue could be extracted using the recon-all function while excluding the lesion area. The area of the lesioning field was estimated as the difference between the reconstruction results before and after coagulation.

## Results

### *Repeatability and comparability study*

To determine whether the PAG is more stable than albumen for further use, we compared the variance of diameters across different coagulations with the same parameters in both phantoms. The difference between the two manipulations of the same protocol in albumen was 1.20 mm ± 1.23 mm, whereas the same value in the PAG was 0.17 mm ± 0.16 mm. The difference between the two groups was statistically significant [ $t(8) = 2.496$ ,  $p = 0.037$ ]. ICCs of the albumen and PAG were 0.760 [95% confidential interval (CI): 0.069–0.944] and 0.992 (95% CI: 0.966–0.998), respectively. Coagulation fields of the PAG and albumen are shown in Supplemental Figure S1. As the power or time increased, the PAG showed a more stable increment, whereas albumen failed to present the power–time related rule.

We further observed the coagulation sizes of the PAG, animals, and humans (Supplemental Figure S3). With the same power of 3 W in 60 s, the coagulation sizes in PAG, animals (in specimen 7 days after the coagulation) and humans (the size of microhemorrhage measured from MRI within 6 h after treatment) were 3.53 mm ± 0.15 mm, 3.80 mm ± 0.14 mm, and 3.63 mm ± 0.15 mm in diameter, respectively. To understand to what extent we should adapt the PAG observations to humans, we additionally compared the PAG with the real-time MRI lesions with the exact permutation test, showing there was no significant difference between the two groups ( $p = 0.33$ ).

### *scRF-TC configurations in vitro*

We performed 3D MRI reconstruction, video analysis, and temperature analysis of coagulations of electrodes with different orientations. During the experiment, in most of the areas with visible

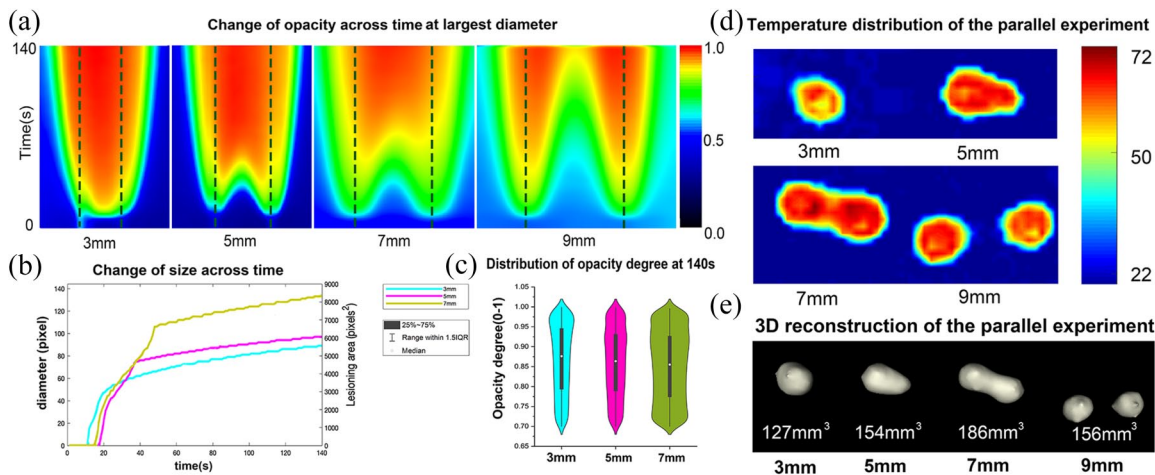


**Figure 3.** Results of coagulation with parallel electrodes of different distances. (a) Change in the degree of opacity across time along the line connecting the two contacts. Here, the opacity degree was defined by setting the value of the opaquest as 1.0, and the value of the most transparent as 0. The dashed lines denote the locations of the contacts. (b) Increase in the diameter along the line connecting the two contacts over time. (c) Statistical distribution of opacity degree 140s after the power was delivered. With increasing distance between the contacts, the degree of opacity decreased, indicating that, with the same power delivered for the same duration, the lesioning field is more extensive, and the coagulation intensity is less extensive. (d) Temperature distribution calculated from machine learning. Most of the temperatures are above 60°C, and only a thin shell of the edge below the temperature is left. (e) 3D MRI reconstruction of the same lesioning field in (d). 3D, three-dimensional; MRI, magnetic resonance imaging.

MRI changes, the temperature of the lesioning field was between 60°C and 78°C.

**Volumes at different distances.** For electrodes in both the parallel (Supplemental video S1) and vertical (Supplemental video S2) arrangements, confluent lesioning fields were created if the distances of the contacts were 3 mm, 5 mm, and 7 mm. The corresponding volumes were 127 mm<sup>3</sup>, 154 mm<sup>3</sup>, and 186 mm<sup>3</sup> for the parallel experiments (Figure 3e) and 130 mm<sup>3</sup>, 165 mm<sup>3</sup>, and 179 mm<sup>3</sup> for the vertical experiments (Figure 4c). At a contact distance of 9 mm, only two small, separate lesioning fields were observed, and the total lesioning volumes decreased to 156 mm<sup>3</sup> for the parallel experiments and 118 mm<sup>3</sup> for the vertical experiments (Figures 3e and 4c). Generally, confluent lesions increased in size as the distance between electrodes increased, but the intensity of coagulation decreased concurrently (Figure 3e).

**Time evolution.** Video analysis of coagulation diameters (Figures 3b and 4b) was further performed in situations where confluent fields were created in both the parallel and vertical experiments. During the coagulation process, lesions

started to become visible at approximately 10–18 s for all electrode distances. For the 3-mm condition, a dense connection was found almost concurrently with the presence of the lesion. However, for electrode distances of  $\geq 5$  mm, a link did not appear immediately, and two tiny, separate, lesions were observed first. The lesions started around each of the contacts and expanded until they merged (Supplemental videos S1 and S2) (Figures 3a and 4a). With the delivery of power, the size of the lesion increased quickly at first, but a drastic change of speed into a plateau could be observed at a specific time (Figures 3b and 4b). Specifically, the time points of the transition of the coagulation diameters were 20 s for 3 mm, 38 s for 5 mm, and 41 s for 7 mm in the parallel trials and 19 s for 3 mm, 26 s for 5 mm, and 52 s for 7 mm in the vertical tests. The transition from a fast-growing state to a plateau state occurred within 1 min when the electrodes were within 7 mm of each other.

**From one contact to multiple contacts.** In this experiment, we evaluated whether one contact could be used for coagulation multiple times with different peripheral contacts, which is essential for modeling a network for coagulation. After the



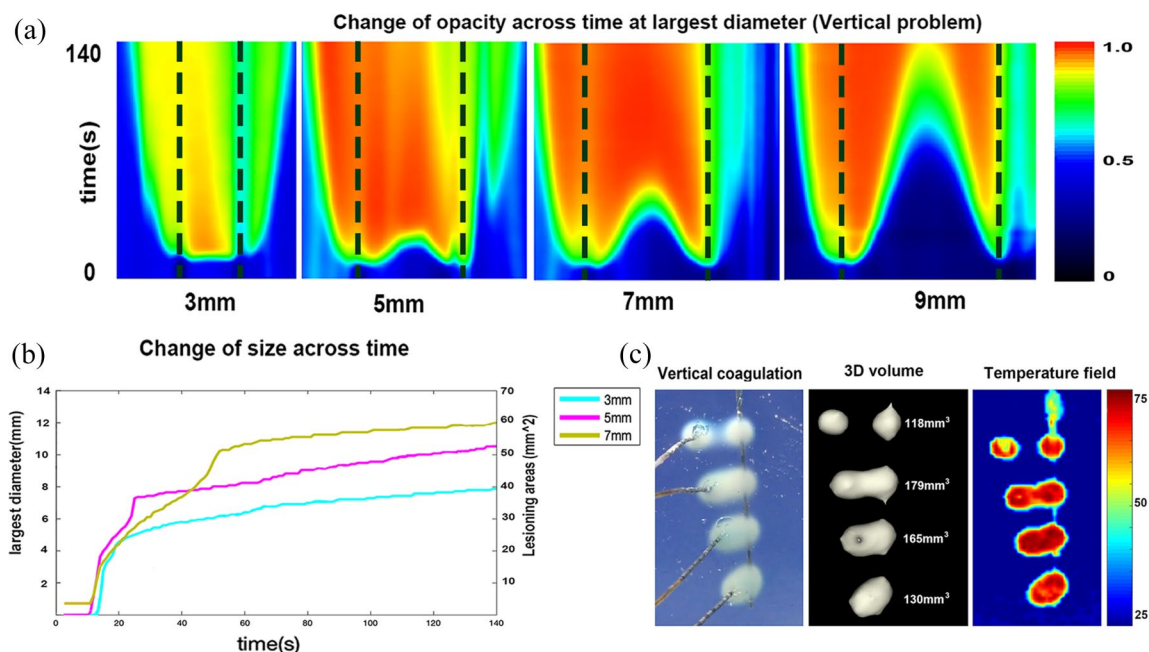


**Figure 4.** Results of coagulation with vertical electrodes of different distances. (a) Change in the degree of opacity over time along the line connecting the two contacts, demonstrating evolution of the lesioning field over time. (b) Increase in the diameter along the line connecting the two contacts over time. As in the parallel experiments, an increase in the distance between the contacts was accompanied by an increase in the lesioning field size. However, the distribution of the degree of opacity was not evaluated here because of the interference of the shadows. A plateau in the diameter increase was also observed. (c) Temperature distribution and 3D MRI reconstruction of the lesioning field. Note that when the distance was  $\leq 7$  mm, the lesioning field is confluent, and the size is increased as the distance between contacts is increased, whereas a decrease in lesion size is observed once the lesioning field becomes separated. 3D, three-dimensional; MRI, magnetic resonance imaging.

RF-TCs, the central contact was reliably connected through the confluent field to all six surrounding contacts, whereas each peripheral contact was connected to two adjacent peripheral contacts and the central contact *via* the confluent area. With parameters of 3 W and 150 s and a contact distance of 7 mm (Supplemental video S3), a single lesioning field with no gaps was created, and MRI 3D reconstruction revealed that the lesion size reached 1823.5 mm<sup>3</sup> (Figure 5). The one-to-multiple experiment resulted in larger lesion volumes than the vertical and parallel experiments.

When the contact distance increased to 9 mm, full coverage was still not realized in the 150-s duration, with only seven islands being created (Figure 5). However, as the central contact underwent 900 s of coagulation (six periods of 150 s for each), facilitated by the sparse distribution of coagulation islands, the long-term radius changes after the transition point (curve of size increment)

could be observed through the central contact (Figure 5). The transition occurred at approximately 140 s; in the subsequent 760 s, the radius had only increased by 1.4-fold from its value at 140 s. Quantitative MRI analysis revealed similar findings. The 3D MRI volume of the lesioning field in the center was only 1.3 times larger than the average volume of the peripheral fields.

#### Effective of the scRF-TC

*scRF-TC and classic RF-TC comparisons in PAG.* Next, we compared the 3D reconstruction volume created by homologous and heterologous coagulations and scRF-TC. When only four contacts were involved (with a period of 3 W for 150 s and contact spacing of 7 mm) (Figure 6), the combined application of both the homologous and heterologous contacts created the most significant coagulation volume (389.31 mm<sup>3</sup>). Heterologous contacts created a lesion of 338.54 mm<sup>3</sup> – 87% of the volume of the most extensive lesion – whereas



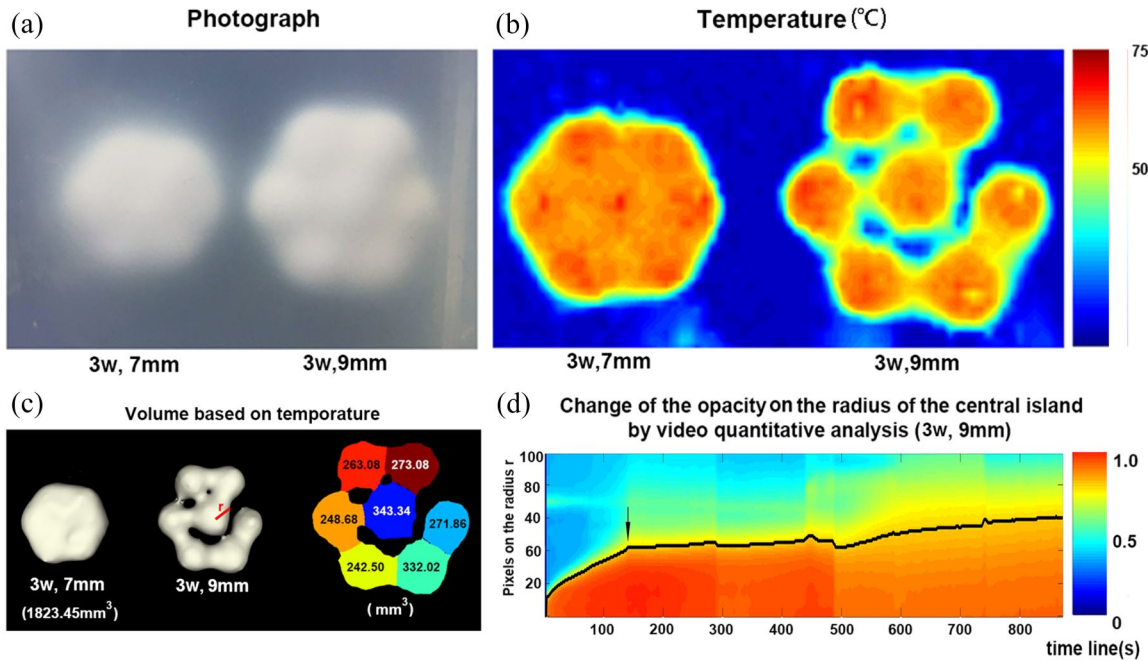


**Figure 5.** Results of the one-to-multiple experiments. (a) Photograph of the coagulation field. (b) Temperature distribution of the same field as in (a). (c) Volumes of the 3D MRI reconstruction of the same field. With 3 W and 7 mm, a confluent coagulation field was created. However, when the distance increased to 9 mm, seven relatively discrete islands were created, and the volume of the central island, which underwent a total of 900-s coagulation, is only 1.3 times the average volume of the peripheral islands (a period 150-s coagulation). (d) As the center island of the lesioning field created with the parameters of 3 W and 9 mm underwent six periods of 150-s coagulations, further video analysis was conducted within the radius  $r$  (red line in c) of the central island to track the evolution of the radius during the total 900-s duration. The black line on the color-coded time-radius map denotes the diameter of the central island (threshold of opacity degree, 0.8). After the transition into the plateau phase, the radius increased by only 1.4-fold during the entire 760-s duration. 3D, three-dimensional; MRI, magnetic resonance imaging.

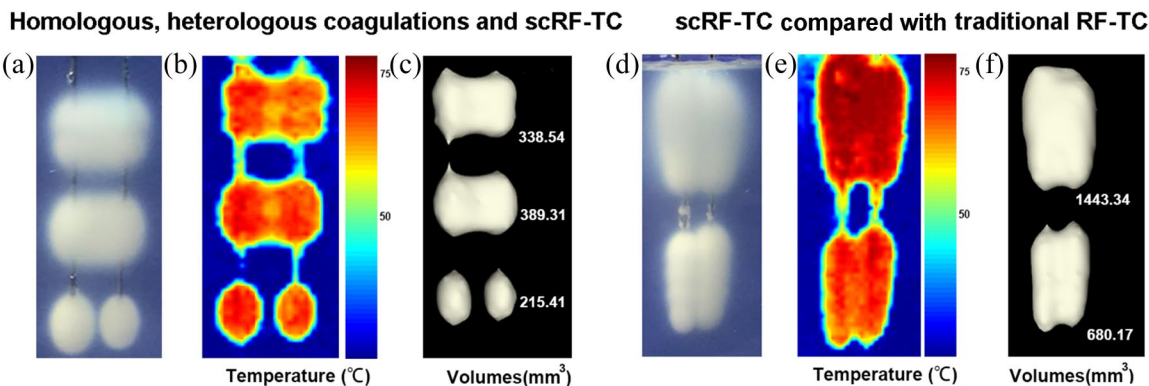


**Figure 6.** Size and temperature analysis of scRF-TC. (a) Field of purely homologous coagulation (bottom), purely heterologous coagulation (middle), as well as the scRF-TC (top) that simultaneously included the heterologous and homologous coagulations. (b, c) Temperature distribution and 3D reconstruction of (a). (d) Field of traditional RF-TC (bottom) and scRF-TC (top), each generated with 10 contacts. (e, f) Temperature distribution and 3D reconstruction of (d). 3D, three-dimensional; MRI, magnetic resonance imaging; RF-TC, radiofrequency thermocoagulation; scRF-TC, stereo-crossed radiofrequency thermocoagulations.

coagulation with only the homologous contacts created the smallest lesion volume (215.41 mm<sup>3</sup>).

As a more conservative electrode distance of 5 mm is typically adopted in clinical practice, to simulate a clinical scenario of consecutive coagulation, we took the following parameters: 3 W, 5 mm, and 150 s. With the involvement of 10 contacts from a pair of parallel electrodes, the scRF-TC, which combined the homologous and heterologous coagulations, created a lesioning field of 1443.34 mm<sup>3</sup>, which was 2.12 times larger than the lesion produced by traditional RF-TC (680.17 mm<sup>3</sup>) (Figure 6).

*Retrospective case.* The retrospective case of a 23-year-old female patient who received the scRF-TC was enrolled. A total of 66 homologous lesioning and 20 heterologous lesioning (12 coagulations were by parallel electrodes, whereas 8 were by vertical electrodes) were performed during the entire process (Figure 2). A total of 26 contacts were involved in the heterologous coagulations, whereas the other contacts were abandoned because of the distribution of vessels or functional areas. Specifically, two contacts in electrode I, the only electrode with a vertical orientation, underwent six periods of coagulations. Among the contacts within the putative epileptogenic zone, an average of 3.46 periods of coagulation was performed. The patient was completely awake, and no complaints were recorded during the coagulation process.

SEEG recordings in the subsequent 45 min suggested complete elimination of active epileptic discharges (Figure 2h). A recheck of MRI within 2 h after coagulation indicated that the lesioning field adequately covered the entire suspected low-metabolism areas (Figure 2a, e, f). The 3D reconstruction demonstrated that the lesioning field was 38.7 cm<sup>3</sup> (blue area in Figure 2f). A 3-month recheck suggested complete absorption of the microhemorrhages. The patient maintained a seizure-free status throughout the following 12 months.

## Discussion

The results of this study indicated that a distance of 7 mm was essential to create a confluent lesioning field regardless of the orientation of the electrodes, and the plateau phase typically appeared within 60 s of duration. Besides, one contact

could create multiple connections with external contacts. These observations indicated that it is practical to create a lesioning network of multiple contacts, or scRF-TC, to create larger coagulation fields. Retrospective clinical observation further demonstrated that, with scRF-TC, the lesioning area was large enough to keep the patient from undergoing a secondary craniotomy, and the patient has been seizure-free since then.

### *Repeatability and comparability of PAG*

We introduced PAG as a phantom of the human brain for RF-TC in the present study. In the past two decades, PAG has been used in areas of thermoablation in other human tissues.<sup>14-17</sup> Regarding SEEG-guided RF-TC in brain tissue, albumen has been used in previous studies.<sup>10,11</sup> After careful comparison of the stability between PAG (ICC: 0.992) and albumen (ICC: 0.760), we found that PAG was more stable, and would be better for further explorations. Besides, albumen was difficult to transport to an MRI scanner, whereas PAG could solve this problem. Concerning the justification of adapting RF-TC results in PAG to those in humans, the present study indicated that, at least at a power of 3 W, the size of the PAG might be presumed as an approximate to the microhemorrhage in humans for further discussion. Experiments in rodents further supported this assumption.

### *Coagulation with different orientation of electrodes*

The results indicated that the orientation of the electrodes should not always be considered as long as the contacts are at proper distances to create a confluent lesioning field. This denotes the feasibility of heterologous coagulations during clinical practice as the electrodes' orientation in patients would typically be customized.

Our observations suggested that when the contacts' distances are in the range of 7 mm or less, the coagulation fields would be confluent. Specifically, with increasing distance of contacts, the volumes are also growing, but the intensity of coagulation was decreasing. Concerning the duration for coagulation, the transition points of the increasing diameters were within 60 s in the quantitative video analysis; this provides evidence that to decrease the total treatment duration of a patient, the lesioning duration of a single

period should be controlled to 60s; thus, we adopted a 60-s period of the scRF-TC to treat the patient. In the confluent coagulation fields of the study, most of the temperatures were between 60°C and 78°C, indicating that promising coagulation of 60°C through the scRF-TC approach is possible.<sup>18</sup>

#### *Coagulation from one contact to multiple contacts*

In the one-to-multiple coagulation experiments, six and three periods of 3 W and 150 s coagulations, respectively, were performed to the central contact and external contacts first; this indicated that the same contact could be used multiple times to create coagulation fields with multiple peripheral contacts. Considering that heterologous coagulation with a different arrangement is possible, we were able to find an appropriate method of creating a network of multiple contacts for further coagulations in 3D space.

We further tried the same coagulation strategy at 150 s and 9 mm. At this time, although only seven islands were created during the 9-mm experiment, we observed that the coagulation size of the central contact increased only 1.3–1.4 times in the subsequent 760 s after the transition point, supporting the previously mentioned point of excluding excessive duration for coagulation after the transition point to shorten the total treatment duration.

#### *Improvement of the lesioning size with scRF-TC*

We compared the volume of scRF-TC, homologous coagulation, and heterologous coagulation with four contacts, and found that scRF-TC created the largest coagulation field. Further observation indicated that heterologous coagulation (created a lesioning field equal to 87% of the lesioning field of scRF-TC) has better performance than the homologous coagulation. Thus, when designing an scRF-TC plan, heterologous coagulation should be used as much as possible, as long as the vessels and eloquent areas are safe.

Regarding the experiment of creating an elongated field with the same number of 10 contacts, the size of the scRF-TC is 2.12 times that of traditional RF-TC, suggesting the possibility of applying scRF-TC to the epileptogenesis that is

in a long shape. Therefore, scRF-TC would be more efficient in creating large lesioning sizes.

#### *Ablating epileptogenesis*

In the patient study, scRF-TC was carried out successfully, and a lesioning volume of 38.7 cm<sup>3</sup> was created. The patient was seizure-free in the following 12 months. According to the pathology literature, the volumes of a medium-sized focal cortical malformation would typically be 20–30 cm.<sup>3,19</sup> The treatment of our patient primarily indicated that, by mini-invasive implantation of electrodes, scRF-TC could ablate a large volume of brain tissues, which previously had to be evacuated by open surgery. Moreover, this process combines the diagnosis and ablation into one procedure and references the multi-modality structural information and electrophysiological signal simultaneously. As the SOZ and the accompanying structural abnormalities should be at different locations,<sup>20,21</sup> the use of scRF-TC could potentially avoid mistreatment.

#### *Limitations*

As the heterologous coagulations of scRF-TC require sufficient distance, more electrodes need to be implanted in scRF-TC than in the traditional SEEG procedure. Typically, partial enhancement of the density is needed by implanting two or three more electrodes to the putative epileptogenesis depending on the size of the lesion, and each implantation of the electrode would result in a 0.08% higher risk of major hemorrhage.<sup>22</sup> However, this risk is still lower than that in open surgery, as the risk of major hemorrhage in open surgery was 1.5%.<sup>23</sup> Again, the cost of additional electrodes could be compensated for by reducing patients' duration of treatment. Yet, although according to the retrospective case, scRF-TC was shown to be practical in creating larger volumes in humans, the 12-month follow up of a single patient is not conclusive enough. Thus, the clinical effectiveness and safety of scRF-TC are still to be validated by cohort studies of larger numbers of sampled cases in the future.

#### **Conclusion**

According to our experiment using PAG, a valid distance for confluent lesioning is 7 mm, regardless of the orientation of the electrodes. The

plateau phase of the lesioning diameters typically starts within 60s of duration. Multiple connections could be created through the same contact. Therefore, creating a network with SEEG electrodes or scRF-TC is practical. This intervention could achieve comprehensive ablation while referencing both structural and electrophysiological information simultaneously with the implantation of SEEG electrodes only.

### Acknowledgments

We thank Hai-Chen Sun (Central Lab, Xuanwu Hospital, Capital Medical University) and Zhi-Ping Zhang (Yasargil Microsurgical Training Center, Department of Neurosurgery, Xuanwu Hospital, Capital Medical University) for the provision of experimental equipment and conditions.

### Availability of data and materials

The data in this study are available from the corresponding author on request.

### Conflict of interest statement

The authors declare that there is no conflict of interest.

### Ethics approval and consent to participate

This study was approved by the ethical committee of Xuanwu Hospital (Approval number: LYS-[2019]-097), and written informed consent to research and publish was obtained from all the four participants involved in the study.

### Funding

The authors disclosed receipt of the following financial support for the research, authorship, and/or publication of this article: This work was supported by the National Key R&D Program of China (grant number: 2016YFC0103909), National Natural Science Foundation of China (grant numbers: 81871009 and 81801288), and Key Project of Beijing Science and Technology Commission (capital characteristics, grant number: Z161100000516008).

### ORCID iD

Yong-Zhi Shan  <https://orcid.org/0000-0001-5510-1026>

### Supplemental material

Supplemental material for this article is available online.


### References

1. Spiegel EA, Wycis HT, Marks M, *et al.* Stereotaxic apparatus for operations on the human brain. *Science* 1947; 106: 349–350.
2. Blume WT, Parrent AG and Kaibara M. Stereotactic amygdalohippocampotomy and mesial temporal spikes. *Epilepsia* 1997; 38: 930–936.
3. Parrent AG and Blume WT. Stereotactic amygdalohippocampotomy for the treatment of medial temporal lobe epilepsy. *Epilepsia* 1999; 40: 1408–1416.
4. Balasubramaniam V and Kanaka TS. Stereotactic surgery of the limbic system in epilepsy. *Acta Neurochir (Wien)* 1976; (23 Suppl): 225–234.
5. Lee CY, Li HT, Wu T, *et al.* Efficacy of limited hippocampal radiofrequency thermocoagulation for mesial temporal lobe epilepsy. *J Neurosurg* 2018; 1: 1–9.
6. Guenot M, Isnard J, Ryvlin P, *et al.* SEEG-guided RF thermocoagulation of epileptic foci: feasibility, safety, and preliminary results. *Epilepsia* 2004; 45: 1368–1374.
7. Cossu M, Fuschillo D, Casaceli G, *et al.* Stereoelectroencephalography-guided radiofrequency thermocoagulation in the epileptogenic zone: a retrospective study on 89 cases. *J Neurosurg* 2015; 123: 1358–1367.
8. Wei PH, An Y, Fan XT, *et al.* Stereoelectroencephalography-guided radiofrequency thermocoagulation for hypothalamic hamartomas: preliminary evidence. *World Neurosurg* 2018; 114: e1073–e1078.
9. Moles A, Guenot M, Rheims S, *et al.* SEEG-guided radiofrequency coagulation (SEEG-guided RF-TC) versus anterior temporal lobectomy (ATL) in temporal lobe epilepsy. *J Neurol* 2018; 265: 1998–2004.
10. Bourdillon P, Isnard J, Catenoix H, *et al.* Stereoelectro-encephalography-guided radiofrequency thermocoagulation: from in vitro and in vivo data to technical guidelines. *World Neurosurg* 2016; 94: 73–79.
11. Staudt MD, Maturu S and Miller JP. Radiofrequency energy and electrode proximity influences stereoelectroencephalography-guided radiofrequency thermocoagulation lesion size: an in vitro study with clinical correlation. *Oper Neurosurg (Hagerstown)* 2018; 15: 461–469.
12. Fan X, Shan Y, Lu C, *et al.* Optimized SEEG-guided radiofrequency thermocoagulation for



- mesial temporal lobe epilepsy with hippocampal sclerosis. *Seizure* 2019; 71: 304–311.
13. Berjano EJ. Theoretical modeling for radiofrequency ablation: state-of-the-art and challenges for the future. *Biomed Eng Online* 2006; 5: 24.
  14. Iizuka MN, Sherar MD and Vitkin IA. Optical phantom materials for near infrared laser photocoagulation studies. *Lasers Surg Med* 1999; 25: 159–169.
  15. Takegami K, Kaneko Y, Watanabe T, *et al.* Polyacrylamide gel containing egg white as new model for irradiation experiments using focused ultrasound. *Ultrasound Med Biol* 2004; 30: 1419–1422.
  16. Iizuka MN, Vitkin IA, Kolios MC, *et al.* The effects of dynamic optical properties during interstitial laser photocoagulation. *Phys Med Biol* 2000; 45: 1335–1357.
  17. Bu-Lin Z, Bing H, Sheng-Li K, *et al.* A polyacrylamide gel phantom for radiofrequency ablation. *Int J Hyperthermia* 2008; 24: 568–576.
  18. Rieke V, Instrella R, Rosenberg J, *et al.* Comparison of temperature processing methods for monitoring focused ultrasound ablation in the brain. *J Magn Reson Imaging* 2013; 38: 1462–1471.
  19. Pascual-Castroviejo I, Hernandez-Moneo JL, Gutierrez-Molina ML, *et al.* Focal cortical dysplasia. Clinical-radiological-pathological associations. *Neurologia* 2012; 27: 472–480.
  20. Luders HO, Najm I, Nair D, *et al.* The epileptogenic zone: general principles. *Epileptic Disord* 2006; 8(Suppl. 2): S1–S9.
  21. Tamilya E, Madsen JR, Grant PE, *et al.* Current and emerging potential of magnetoencephalography in the detection and localization of high-frequency oscillations in epilepsy. *Front Neurol* 2017; 8: 14.
  22. González-Martínez J, Bulacio J, Thompson S, *et al.* Technique, results, and complications related to robot-assisted stereoelectroencephalography. *Neurosurgery* 2015; 78: 169–180.
  23. Algattas H, Kimmell KT and Vates GE. Risk of reoperation for hemorrhage in patients after craniotomy. *World Neurosurg* 2016; 87: 531–539.

Visit SAGE journals online  
[journals.sagepub.com/  
 home/tan](http://journals.sagepub.com/home/tan)

 SAGE journals